https://doi.org/10.3847/1538-4357/aba268

On the Magnetospheric Origin of Repeating Fast Radio Bursts

Wei-Yang Wang[1,2,3] ⓘ, Renxin Xu[3,4,5] ⓘ, and Xuelei Chen[1,2,6] ⓘ

[1] Key Laboratory for Computational Astrophysics, National Astronomical Observatories, Chinese Academy of Sciences, 20A Datun Road, Beijing 100101, People's Republic of China; wywang@bao.ac.cn, xuelei@cosmology.bao.ac.cn
[2] University of Chinese Academy of Sciences, Beijing 100049, People's Republic of China
[3] School of Physics and State Key Laboratory of Nuclear Physics and Technology, Peking University, Beijing 100871, People's Republic of China
[4] Kavli Institute for Astronomy and Astrophysics, Peking University, Beijing 100871, People's Republic of China
[5] Department of Astronomy, School of Physics, Peking University, Beijing 100871, People's Republic of China
[6] Center for High Energy Physics, Peking University, Beijing 100871, People's Republic of China

Abstract

A bright radio burst was newly discovered in SGR 1935+2154, which exhibits some fast radio burst (FRB)-like temporal and frequency properties, suggesting a neutron star (NS)/magnetar magnetospheric origin of FRBs. We propose an explanation of the temporal and frequency properties of sub-pulses of repeating FRBs based on the generic geometry within the framework of charged-bunching coherent curvature radiation in the magnetosphere. The sub-pulses in a radio burst come from bunches of charged particles moving along different magnetic field lines. Their radiation beams sweep across the line of sight at different times, and those radiating at the more curved part tend to be seen earlier and at higher frequency. However, by considering bunches generated at slightly different times, we find there is also a small probability that the emission from the less curved part can be seen earlier. We simulate the time–frequency structures by deriving various forms of the electric acceleration field in the magnetosphere. This structure of sub-pulses is a natural consequence of coherent curvature radiation from an NS/magnetar magnetosphere with suddenly and violently triggered sparks. We apply this model to explain the time–frequency structure within a specific dipolar configuration by invoking the transient pulsar-like sparking from the inner gap of a slowly rotating NS, and we have also applied it to more generic configurations.

Unified Astronomy Thesaurus concepts: Radio transient sources (2008); Magnetars (992); Neutron stars (1108); Radio bursts (1339); Non-thermal radiation sources (1119)

1. Introduction

Fast radio bursts (FRBs) are mysterious millisecond-duration astronomical radio transients with large dispersion measures (DMs) and extremely high brightness temperatures (Lorimer et al. 2007; Keane et al. 2012; Thornton et al. 2013; Kulkarni et al. 2014; Masui et al. 2015; Petroff et al. 2015, 2016; Spitler et al. 2016; Chatterjee et al. 2017). The excess of galactic DMs and localization of the host galaxies for several FRB sources shed light on the cosmological origins of FRBs (Bassa et al. 2017; Chatterjee et al. 2017; Marcote et al. 2017, 2020; Tendulkar et al. 2017; Bannister et al. 2019; Prochaska et al. 2019; Macquart et al. 2020). Some FRBs have been found to be repeating, and a very intriguing time–frequency structure has been found (Caleb et al. 2019; CHIME/FRB Collaboration et al. 2019a, 2019b; Hessels et al. 2019; Josephy et al. 2019; Chawla et al. 2020; Fonseca et al. 2020; Luo et al. 2020) in some of the repeating FRBs. For these bursts, each has several sub-pulses with narrowband and different central frequencies, arriving at the detector at different times. For most of them, the time–frequency structure shows a downward-drifting pattern, i.e., the later-arriving sub-pulses have lower frequencies. There are some possible upward-drifting tendencies shown on MJD 58720, burst 191219 A & B, as well as in the bright and faint sub-pulses in burst 191219 B of FRB 180916.J0158+65 (Chawla et al. 2020; The CHIME/FRB Collaboration et al. 2020). We have proposed a model by invoking a sudden-trigger-excited coherent curvature radiation in a neutron star (NS) magnetosphere to explain the downward-drifting pattern (Wang et al. 2019).

Very recently, a two-component bright radio burst with FRB-like temporal and frequency properties was detected by the Canadian Hydrogen Intensity Mapping Experiment (CHIME; Scholz & Chime/Frb Collaboration 2020; CHIME/FRB Collaboration et al. 2020) and the Survey for Transient Astronomical Radio Emission 2 (STARE2; Bochenek et al. 2020a, 2020b) during the active state of the Galactic magnetar SGR 1935+2154, leading to the NS/magnetar magnetospheric origin of FRBs. An X-ray burst detected by several X-ray instruments such as AGILE (Tavani et al. 2020), Insight-HXMT (Li et al. 2020; Zhang et al. 2020a, 2020b), INTEGRAL (Mereghetti et al. 2020), and Konus-Wind (Ridnaia et al. 2020), exhibits two hard peaks separated by ~30 ms, in temporal coincidence with the radio burst event. Following-up deep searches by the Five-hundred-meter Aperture Spherical Telescope (FAST) revealed no FRB detection during the epochs that 29 soft γ-ray bursts were detected by Fermi (Lin et al. 2020), suggesting the SGR-associated radio burst event is very rare. The FRB-like time–frequency structure of the radio burst is reminiscent of sub-pulse drifting, which is a well-known phenomenon in some normal radio pulsars (Rankin 1986) and is explained as $E \times B$-induced drift in an NS magnetosphere (Ruderman & Sutherland 1975). The consecutive sparking process in the polar cap region of a normal radio pulsar would give rise to regular drifting of sub-pulses, while the repeating FRB sources and the SGR 1935+2154 bursts are more akin to a sudden and violent sparking process. Models of this suddenly triggered mechanism in the magnetosphere of an NS/magnetar to account for FRBs have been proposed by many authors (e.g., Connor et al. 2016; Cordes & Wasserman 2016; Dai et al.

2016; Katz 2017; Zhang 2017; Wang et al. 2018; Wadiasingh & Timokhin 2019).

Motivated by the intriguing time–frequency structures in repeating FRBs and the FRB-like radio burst of SGR 1935 +2154, in this paper we expand the Wang et al. (2019) model to explain the behaviors of suddenly and violently triggered sparks in the magnetosphere, by deriving the dynamics of particle bunches. The model is demonstrated in Section 2, and its applications in several scenarios are discussed in Section 3. The results are summarized in Section 4 with some discussions.

2. The Magnetospheric Model

If the size of the charged particle bunch is less than half a wavelength (for 1 GHz, $\lambda/2 \sim 10$ cm) or smaller, the phase of radiation from the particles is approximately the same, which allows the production of coherent radio emission. In several models the FRBs are interpreted as coherent radio emission from charged particle bunches in pulsar magnetospheres (Katz 2014; Kumar et al. 2017; Lu & Kumar 2018; Yang & Zhang 2018; Lu et al. 2020). We consider the coherent curvature radiation whose frequency reads $\nu = (3/4\pi)\, \gamma^3\, (c/\rho)$, where γ is the Lorentz factor of the emitting particles, c is the speed of light, and ρ is the curvature radius. The observed narrowband sub-pulses can be interpreted as a part of a multisegment broken power-law spectrum for bunching coherent curvature radiation from charge-separated clumps (Yang et al. 2020). The observed sub-pulse frequency is determined by both the geometric conditions and the dynamics of the emitting particles.

2.1. The Geometry

We evolve the previous model proposed by Wang et al. (2019) which invokes bunching coherent curvature radiation in an NS magnetosphere. A sudden trigger can let the NS become active for several milliseconds or longer. During the active state, many sparking events may occur, e.g., via sudden magnetic reconnection or NS crust cracking. Bunches of electron–positron pairs are created by these sparking mechanisms, move along the curved field lines, and process charge separation by an electric field parallel to the magnetic field lines. The decoupled and charge-separated bunches, e.g., positron clumps, stream outward along the open field lines, producing coherent curvature emissions. We define the sub-pulses as emissions from these bunches produced by sparking events during the same trigger. Magnetic field lines sweep across the line of sight (LOS) as the magnetosphere rotates. Only the bunches that arrive at their emission points where they also happen to sweep the LOS can be observed by us. The observer can see the emission from several sporadic bunches of neighboring magnetic field lines, as shown in Figure 1.

Basically, the motion of the bunches along the field lines includes both outflow and corotation with the NS in the magnetosphere simultaneously. Therefore, one can calculate the time delay either via the projected horizontal motion, e.g., phase delay (Wang et al. 2019) or via the geometry of outflow (this work). The observed time delay of the two sub-pulses is generically given by

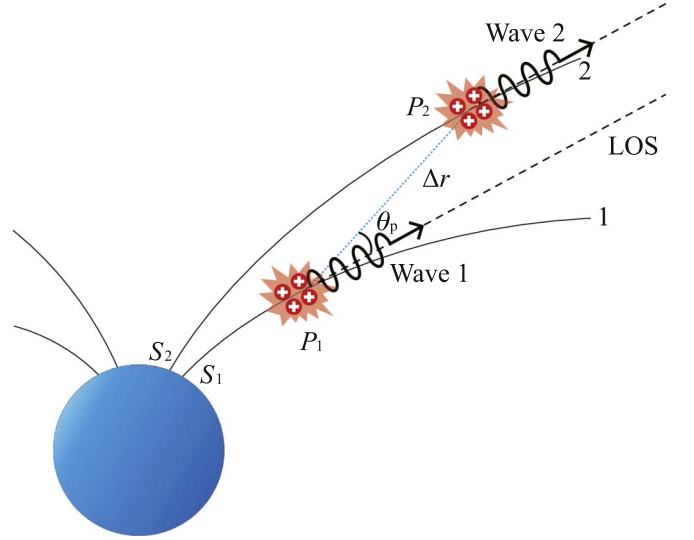$$\Delta t_{\text{obs}} = \frac{d_2 - d_1}{c} + t_{P_2} - t_{P_1}, \quad (1)$$

Figure 1. Schematic diagram of the neutron star/magnetar magnetosphere and radiation particle bunches. As an example, two magnetic field lines with charged bunch stream outflows are plotted. The dashed lines show the line of sight (LOS). P_1 and P_2 denote the points where emissions can sweep the LOS at two magnetic field lines, i.e., two emitting points. Here, we assume that the curvature radius at P_1 is smaller than that at P_2. The points S_1 and S_2 denote the locations where the two bunches are generated.

where d_1 and d_2 are the distance of the two emitting points from us, and t_{P_1} and t_{P_2} are the times when the bunches arrived at their respective emitting points. The observed emissions can be created by the bunches which are excited at different times. By deriving the motion of bunch outflow, one can generally write

$$t_{P_1} = t_{10} + \frac{s_1}{v_e}, \qquad t_{P_2} = t_{20} + \frac{s_2}{v_e}, \quad (2)$$

where t_{10} and t_{20} are the times when those bunches were generated, s_1 and s_2 are the distances that the bunches traveled from the generation points to the emitting points along the field lines, and $v_e = \beta_e\, c$ is the velocity of the bunch particles. Combined with Equations (1) and (2), one can obtain

$$\Delta t_{\text{obs}} = \Delta t_{\text{geo}} + t_{20} - t_{10}, \quad (3)$$

where Δt_{geo} is the geometric time delay, which can be written as

$$\Delta t_{\text{geo}} = \frac{s_2 - s_1}{v_e} - \frac{\Delta r \cos \theta_p}{c}, \quad (4)$$

where $\Delta r \cos \theta_p$ is the projection of the distance between the two emitting points in the direction of the LOS.

According to Equation (3), if two bunches are generated simultaneously, their emissions would be observed at different epochs. In this case, the emission from the more curved part (line 1) is seen earlier than that from the less curved (line 2). On the other hand, the emission from line 2 may arrive the detector at an earlier time if the bunch was generated much earlier. For the geometry-dependent plasma emission mechanism, one would observe different time–frequency structures from some sub-pulses.

2.2. Acceleration of Charged Particles

An electric field $E_\parallel$ parallel to the B-field that sustains the acceleration of charged particles is required, otherwise the particles will cool down very rapidly (Kumar et al. 2017). $E_\parallel$ can accelerate bunches of electrons and positrons to ultra-relativistic velocities moving in opposite directions. The acceleration of the charged bunches can be written as

$$N_e E_\parallel eds - L dt = N_e m_e c^2 d\gamma, \tag{5}$$

where N_e is the number of positrons in the bunches, L is the total luminosity of the radiation, and m_e is the positron mass. In order to sustain a constant Lorentz factor within a lab-frame duration of γ^2/ν, i.e., balance between acceleration and radiation cooling, one requires $E_{\parallel,0}$ (Wang et al. 2019) given by

$$E_{\parallel,0} \simeq \frac{\gamma m_e c}{(e t_{cool})} \sim 3.1 \times 10^7 \nu_9^2 N_{e,23} \gamma_2^{-2} \text{ esu}, \tag{6}$$

where we adopt the convention $Q_x = Q/10^x$ in cgs units. If the strength of $E_\parallel$ is much stronger than $E_{\parallel,0}$, Equation (5) can be approximated as

$$E_\parallel e \beta_e dt \simeq m_e c d\gamma. \tag{7}$$

Many trigger mechanisms have been proposed to explain FRBs (see Platts et al. 2019 for a review). One possible scenario is that the $E_\parallel$ may be triggered together with the bunch generation. We investigate a list of possible trigger mechanisms that might create $E_\parallel$ in the magnetosphere.

(1) Crustal deformation-triggered field via Alvén waves in the charge starvation region (Kumar & Bošnjak 2020). The Alvén waves can be created by a sudden crustal motion, starquake, or emergence of magnetic flux tubes (e.g., Wang et al. 2018; Wadiasingh & Timokhin 2019), and then propagate in the inhomogeneous magnetosphere. The timescale for this process can be estimated as $\sim R/v_A \approx 0.3$ s, where R is the radius of the NS surface and v_A is the Alvén speed adopted as $0.01c$. An electric field is formed in the charge starvation region, since the plasma is insufficient to supply the current needed by the Alvén wave. The acceleration field is described as (Kumar & Bošnjak 2020)

$$E_\parallel = E_d \sin[\omega_{aw}(s/c - t)], \tag{8}$$

where ω_{aw} is the angular frequency of the Alvén wave and E_d is the field that provides displacement current given by

$$E_d = -(k_{aw\perp}/k_{aw\parallel})\delta B \propto r^{-3}. \tag{9}$$

If the Alvén wave oscillates not so rapidly, e.g., the phase term $\sim -10^{-2}\omega_{aw,5}t_{-3}\gamma_2^{-2}$, the acceleration for charged bunches is mainly determined by the power-law component.

(2) A self-induced field in the twist current-carrying bundle (Beloborodov & Thompson 2007). When the star undergoes a sudden crust quake, the motion of footpoints can cause the outer magnetosphere to twist up. During this process, the ejected currents flow along the field lines to the exterior of the star and come back at other footpoints, supporting the twisted magnetic field. $E_\parallel$ is generated by the self-induction of the current, which can be written as

$$E_\parallel \simeq \frac{c\tau B \sin^2\theta \Delta\phi}{r} \propto r^{-4}, \tag{10}$$

where τ is the timescale of the current dissipation, B is the magnetic field strength, and $\Delta\phi$ is the twist angle.

(3) The "cosmic comb" model (Zhang 2017). A plasma stream from a nearby source (e.g., binary companion or massive black hole, etc.) causes the NS to interact with the ram pressure, overcoming the magnetic pressure. The sudden distortion of the magnetosphere can cause the number density to deviate from the original Goldreich–Julian value, forming bunches of charged particles in a locus of field lines. $E_\parallel$ is created due to the sudden compression of the Goldreich–Julian density. For an easy illustration, we relate the deviation of the net charge density to the original Goldreich–Julian density, i.e., $\xi B/(Pce)$, where ξ is the compression factor and P is the period. Thus, one has $\nabla \cdot E_\parallel \simeq 4\pi\xi B/(Pc)$. Combined with the boundary condition of $E_\parallel = 0$ at $r \gg cP/(2\pi)$, the acceleration field is given by

$$E_\parallel \simeq \frac{2\pi\xi Br}{Pc} \propto r^{-2}. \tag{11}$$

On the other hand, in order to derive a constant Lorentz factor, the required electric field reads (Wang et al. 2019)

$$E_{\parallel,0} \simeq \frac{8\pi\mu\eta_c Br}{27\gamma^2\lambda} \propto r^{-2}, \tag{12}$$

where μ is the normalized fluctuation of electrons and η_c is a parameter describing the cross section.

The $E_\parallel$ proposed in these models can all be written in a power-law form, but differ in their indices. Another possible scenario for $E_\parallel$ is that it is the acceleration field in the slot gap above the pulsar polar caps (Arons 1983).

2.3. Drifting Parttern

Similar to normal pulsars, the drifting pattern of FRBs can reflect the emitting conditions changing with the locations at the magnetosphere (e.g., "radius-to-frequency mapping"; Lyutikov 2020). The drift rate can be written as

$$\dot\nu = \nu\left[3\frac{\Delta\gamma}{\gamma\Delta t_{obs}} - \frac{\Delta\rho}{\rho\Delta t_{obs}}\right]. \tag{13}$$

If $E_\parallel$ is very close to $E_{\parallel,0}$, the Lorentz factors of the bunches will be the same for each and will not evolve significantly as they stream out along the field lines; therefore the drift rate can be simplified as

$$\dot\nu = -\nu\frac{\Delta\rho}{\rho\Delta t_{obs}}. \tag{14}$$

The drift rate is mainly determined by the change of curvature radius of the emitting points. Generally, the emitting points that swept the LOS earlier emit curvature radiation in the more-curved part of the field lines, resulting in downward-drifting patterns. On the other hand, if the two bunches are not triggered simultaneously, e.g., the bunch at line 2 is generated earlier than that at line 1, from Equation (3) the wave from the line 2 could be observed earlier when $|t_{20} - t_{10}|$ is longer than t_{geo}, so that an upward-drifting pattern will be seen. For the scenario $E_\parallel \gg E_{\parallel,0}$, the drift rate can be influenced by the difference in γ for the bunches at different field lines. A complex drifting pattern may be caused by a complicated $E_\parallel$.

3. Applications

We apply this radiation model to two scenarios. In the first scenario, the magnetic field configuration is a simple dipole, pulsar-like sparking process generating bunches of charged particles at the inner gap region; FRBs are subsequently produced in the polar gap region at the open field lines. The second scenario is more generic; here we do not specify the trigger mechanism, just give a generic field line configuration. The sparking process can be caused by either internal or external excitation.

3.1. Polar Gap Sparking in a Dipole Field

We consider a scenario similar to the polar gap sparking of normal radio pulsars (Ruderman & Sutherland 1975). The mechanism we envisage here is a sudden and violent sparking process to produce bunches at the stellar surface. When the sudden sparking perturbs the magnetic field to deviate significantly from the regular state, bunches of charged particles will produce coherent curvature radiation in a locus of field lines (Yang & Zhang 2018). Multiple bunches emitting in adjacent field lines traveling with a similar initial Lorentz factor as the perturbation propagate outwards as Alfvén waves.

In spherical coordinates (r, θ, ϕ) with respect to the magnetic axis, a magnetic field line of the dipolar configuration can be described as

$$u = \frac{R \sin^2 \theta}{r} = \sin^2 \theta_s, \qquad (15)$$

where u is a dimensionless constant and θ_s is the angle of the footpoint for each field line at the stellar surface. For a field line characterized by u, the distance along the field from θ_0 to θ is given by

$$s = \frac{R}{u} \int_{\theta_0}^{\theta} \sqrt{1 + 3\cos^2 \theta} \, \sin\theta d\theta. \qquad (16)$$

The polar gap region is enclosed within the last open field lines, and has a polar angle $\theta_c = 0.1(P/10 \text{ ms})^{-1/2}$. In order to have coherent emission, the bunch opening angle should be smaller than $1/\gamma$, suggesting $P > 0.3 \text{ s}(\gamma/300)\Delta t_{\text{obs}}$ (Wang et al. 2019). As shown in Figure 1 in line 1 and line 2 are in the same plane approximately, i.e., rotation effects (Lyutikov 2020) can be neglected. Therefore, we obtain $\theta_c < 0.02(\gamma/300)^{-1/2}$. Within the region $\theta \lesssim 0.5$, Equation (16) can be approximated as

$$s \simeq \frac{2R}{u}(\cos\theta_0 - \cos\theta) \simeq r. \qquad (17)$$

From Equation (4), the geometric time delay can be written as

$$\Delta t_{\text{geo}} \simeq \frac{\Delta r}{c}\left(1 - \cos\theta_p + \frac{1}{2\gamma^2}\right). \qquad (18)$$

The curvature radius of the field line can be also described as $\rho \approx 4r/(3\sin\theta)$.

We assume that the Lorentz factor is a constant, and first consider that the bunches are generated at the same time. Combining Equations (14) and (18), the drift rate can be
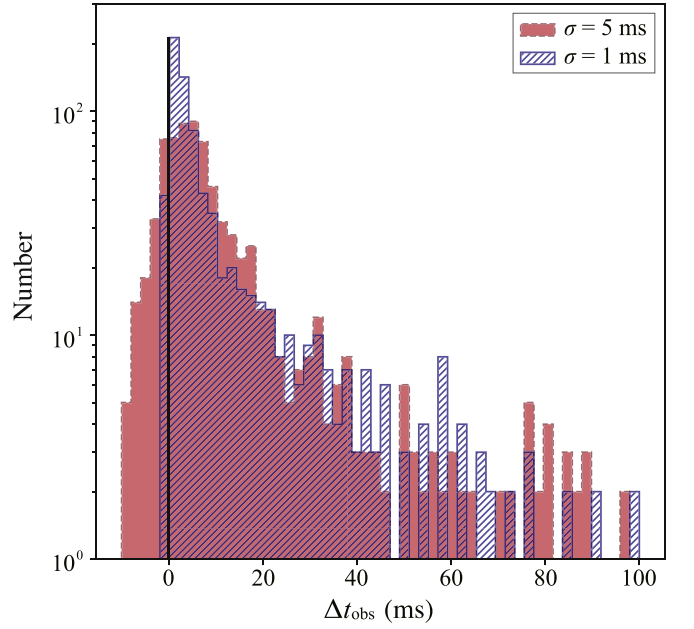

Figure 2. Histograms of estimated Δt_{obs} from Equation (3). The time delay due to the non-simultaneous sparking is assumed as a Gaussian distribution with $\mu = 0$ and $\sigma = 1$ ms, (blue) 5 ms (red). Δt_{geo} is simulated by having $\sin\theta_s$ uniformly distributed when θ_s varies in the range 0–0.02. The vertical black solid line divides events with positive/negative values.

calculated as

$$\dot\nu = -\nu^2 \frac{16\pi}{9\gamma^3(1 - \cos\theta_p + 1/2\gamma^{-2})\sin\theta}. \qquad (19)$$

The luminosity of the coherent curvature radiation reads $N_e^2 \delta p_e$, where δp_e is the luminosity for one electron/positron. From Equation (5), to sustain a constant Lorentz factor, one requires the acceleration field to obey the function $E_{\parallel,0} \propto \rho^{-2}$.

We now consider that bunches are produced at different times. This may be due to the rough surface of a pulsar (Lu et al. 2019), and the binding energy of particles on stellar surface needs to be very high (e.g., in a bare NS with no gaseous atmosphere sitting on top of the crust (Turolla et al. 2004) or solid strangeon star (Xu et al. 1999; Yu & Xu 2011)). The distance between the two emitting points can be written as

$$\Delta r = \frac{-2R\sin^2\theta\cos\theta_s\Delta\theta_s}{\sin^3\theta_s}. \qquad (20)$$

Thus, the geometric time delay is estimated as

$$\Delta t_{\text{geo}} \simeq 6.7 \times 10^{-2} \text{ ms } \theta^2 \Delta\theta_s \sin^{-3}\theta_s(1 - \cos\theta_p). \qquad (21)$$

To assess the overall time–frequency structure of the bursts in this model, we make a simulation of the bursts. We adopt a uniformly distributed $\sin\theta_s$ in the range 0–0.02, $\theta = 0.1$ and $\Delta\theta_s = 0.01$ rad in the simulation. The term $1 - \cos\theta_p \simeq 1$ is assumed. The term $t_{20} - t_{10}$ follows the normal distribution with $\mu = 0$ and $\sigma = 1$ ms, 5 ms. Based on Equation (3), we plot the simulated distribution of the observation interval time Δt_{obs} with 1000 samples, as shown in Figure 2. The temporal properties of the simulated patterns are consistent with the observations from most repeating FRBs. The vertical black solid line divides positive/negative slope values. According to our simulation, in most cases one would observe a downward-drifting pattern, though there are also cases in which an
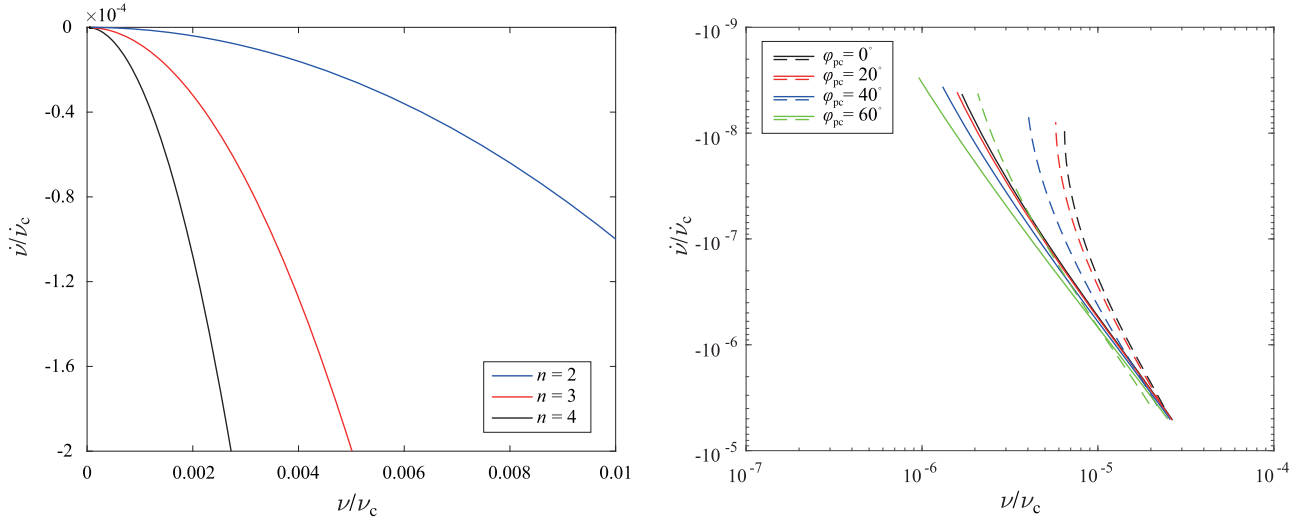
Figure 3. Drift rate as a function of emission frequency. Both the frequency and drift rate are normalized to their characterized parameters. Left: simulated drifting patterns for power-law-distributed $E_\parallel$ are plotted as solid lines with $n = 2$ (blue), $n = 3$ (red), and $n = 4$ (black). Right: same as left but for $E_\parallel$ in the slot gap with $\theta_c = 0.02$. Patterns with different inclination angles are plotted as solid lines ($\alpha = 10°$), and dashed lines ($\alpha = 30°$) ($\alpha = 50°$) for $\phi_{pc} = 0°$ (black), $\phi_{pc} = 20°$ (red), $\phi_{pc} = 40°$ (blue), and $\phi_{pc} = 60°$ (green).

upward-drifting pattern will be seen. As the value of σ increases, the probability of upward drifting will also increase and gradually tend to 50%.

Different trigger mechanisms may lead to various forms of the accelerating electric field $E_\parallel$. For the mechanisms mentioned in Section 2.2, it has a power-law form, i.e., $E_\parallel = E_0(r/R)^{-n}$, when $E_\parallel \gg E_{\parallel,0}$. Different power-law indices reflect different trigger mechanisms. From Equation (13), the drift rate can be written as

$$\dot{\nu} = \frac{9E_0^3 e^3 R \sin\theta}{16\pi m_e^3 c^4 (1 - \cos\theta_p + 1/2\gamma^{-2})} C_n(\eta), \qquad (22)$$

where $\eta = r/R$, which is assumed to be much larger than 1, and $C_n(\eta)$ is given by

$$C_n(\eta) = \begin{cases} \dfrac{[(2 - 3n)\eta^{1-n} + 1](\eta^{1-n} - 1)^2}{(1 - n)^3 \eta^2}, & n \neq 1 \\ \dfrac{3[\mathrm{Log}_e(\eta)]^2 - [\mathrm{Log}_e(\eta)]^3}{\eta^2}, & n = 1 \end{cases}. \qquad (23)$$

The drift rate and the emission frequency are normalized to

$$\dot{\nu}_c = (9E_0^3 e^3 R \sin\theta) \big/ [16\pi m_e^3 c^4 (1 - \cos\theta_p + 1/2\gamma^{-2})],$$

and

$$\nu_c = 9E_0^3 e^3 R^2 \sin\theta / (16\pi m_e^3 c^5).$$

In Figure 3, we show the simulated drift rate as a function of emission frequency for different values of n. More generally, the sign of the drift rate depends on n. As shown in Equation (23), as the acceleration of the electric fields decreases with r rapidly ($n \gtrsim 1$), the growth of the Lorentz factor at greater height is slow, so that frequencies may drift from high values to low. If n is much larger than 1, the drift pattern is approximately $\dot{\nu} \propto -\nu^2$. For $n \lesssim 1$, the Lorentz factor at greater height is much larger, therefore both downward and upward drifting are possible.

For the slot gap, $E_\parallel$ has a more complex form. The slot gap region is bounded by the last open field lines and the magnetic

co-latitude lines. In this region, the combination of geometrical screening and the effect of frame dragging can give rise to a regime of extended acceleration for charged particles, with the acceleration rate

$$\frac{d\gamma}{ds} \simeq A\left(\frac{\kappa}{\eta^4}\cos\alpha + \frac{\theta_c}{4}\eta^{-1/2}\sin\alpha\cos\phi_{pc}\right), \qquad (24)$$

where A is a factor, $\kappa = 0.15$ is the general relativistic parameter entering the frame-dragging effect, α is the inclination angle, and ϕ_{pc} is the magnetic azimuthal angle (Muslimov & Harding 2003, 2004). Here, we set $E_0 = A m_e c^2/e$. From Equation (13), the drift pattern reads

$$\nu = \frac{\nu_c}{\eta}\left[\frac{\theta_c}{2}(\eta^{1/2} - 1)\sin\alpha\cos\phi_{pc} - \frac{\kappa}{3}(\eta^{-3} - 1)\cos\alpha\right]^3 \qquad (25)$$

and

$$\dot{\nu} = \frac{\dot{\nu}_c}{\nu_c}\left(\frac{d\nu}{d\eta}\right). \qquad (26)$$

In Figure 3, we plot the drifting patterns for bunches accelerated by $E_\parallel$ in the slot gap with different parameters. All the patterns show downward-drifting structures. However, for a larger θ_c \$, upward-drifting structure is possible because $E_\parallel$ decrease not so rapidly that Lorentz factors at greater height are large, leading to high-frequency waves.

Both mechanisms give rise to field strength decay with height, so that $E_\parallel$ at the higher region is close to $E_{\parallel,0}$. Thus, the drifting pattern tends to $\dot{\nu} \propto -\nu^2$ at lower-frequency bands.

3.2. A Generic Field Configuration

In this generic model, we consider that the magnetic fields deviate from a simple dipole. For instance, a possible scenario is a highly twisted magnetosphere of a magnetar, e.g., Thompson & Duncan (1995). The pulsar-like sparking process invoked here is similar to the case discussed in Section 3.1 but electron–positron pairs are created via two-photon-pair

production. Another scenario is that the magnetosphere is combed by a plasma stream (Zhang 2017). The sudden trigger can cause the number density to deviate, forming sparks in a locus of field lines and providing acceleration for the charged bunches.

For the generic model, the magnetic field can be generally written as $\boldsymbol{B}(B_r, B_\theta, B_\phi)$. Then we implement the following procedure.

(1) Define the geometry of field lines via $B_r/B_\theta = dr/(rd\theta)$ and $B_\theta/B_\phi = d\theta/(\sin\theta d\phi)$.
(2) Find the positions of bunch generation and emitting point at each field line.
(3) Calculate the distances that the bunches traveled from the generation points to the emitting points along the field lines.
(4) Derive the observed time delay from Equation (3).
(5) Find $E_\parallel$ in the magnetosphere during the trigger.
(6) Calculate the Lorentz factors from Equation (5).
(7) Combining the geometry of the field configuration and the dynamics of emitting bunches, derive the drifting pattern from Equation (13).

4. Summary and Discussion

We propose a generic geometrical mechanism to explain the temporal and frequency properties of sub-pulses of repeating FRBs within the framework of coherent curvature radiation in the magnetosphere of an NS/magnetar. The bunches of charged particles are produced by suddenly and violently triggered sparks from the magnetosphere, and stream outwards along the open field lines. The observed sub-pulse emission can then be interpreted as the emission from several sporadic bunches of neighboring magnetic field lines. This model is applied to explain the time–frequency structure within a specific dipolar configuration by invoking sparking from the inner gap of a slowly rotating NS, and is also developed in more generic configurations. For an NS with sudden and violent triggered sparking, this structure of sub-pulses is a natural consequence of coherent curvature radiation from sporadically observed bunches. We further argue that this structure could be regarded as evidence of the magnetospheric origin of FRBs. We expect to test this FRB model of magnetospheric origin in the future with advanced facilities, especially FAST (Jiang et al. 2019), which has great advantages in detecting faint radio bursts, and CHIME in detecting more FRB samples (CHIME/FRB Collaboration et al. 2018).

The temporal and frequency properties of sub-pulses are supposed to be strongly related to the geometry of the magnetosphere and the dynamics of charged particles within it. In principle, a complicated time–frequency structure could originate from a very complex magnetosphere or the accelerating electric field. The simplest scenario is that these bunches are triggered simultaneously, and move with a nearly constant Lorentz factor, suggesting the potential observation of a $\dot\nu \propto -\nu^2$ relation. The time interval between two adjacent sub-pulses should be longer for lower-frequency emissions because they are emitted at greater height. Sub-pulses with short intervals are more likely to be observed in higher-frequency bands.

A more complex case is that the bunches are generated at slightly different times. We simulated the observed intervals of

sub-pulses in a dipole magnetic configuration. We found in most cases that the emissions from the more-curved parts of the field lines are seen earlier than those from the less-curved parts. As shown in Figure 2, more events with $\Delta t_{\rm obs} < 0$ can occur for larger σ, suggesting that the long-duration trigger mechanism is more likely to generate upward-drifting events. For a long enough trigger event, the chance of observing upward and downward drifting should be the same. Our model model predicts that most FRBs would have downward-drifting sub-pulses, but there are also upward-drifting events, and one would be more likely to observe these from FRBs with long duration.

Most repeating FRBs have same order of drift rates at 400–800 MHz (CHIME/FRB Collaboration et al. 2019a, 2019b; Fonseca et al. 2020), suggesting that FRB sources most likely have similar magnetospheres. This similarity is also enhanced by the measurement of drift rates at ∼1 GHz for FRB 121102 and FRB 181123 (Zhu et al. 2020). For FRB 121102, the drift rates of bursts detected in the higher-frequency band are generally larger than those in the lower-frequency band (Caleb et al. 2019; Hessels et al. 2019; Josephy et al. 2019), matching the scenario of a rapidly decreasing $E_\parallel$.

A pulsar or magnetar, when excited by a sudden trigger to create sporadic sparks, may be seen to have such sub-pulse structures within some single transient pulses. The sudden trigger for a normal pulsar may be related to abrupt crust cracking, which should be accompanied by glitches (Ruderman et al. 1998). Magnetars can create sparks via magnetospheric twist and become active (Beloborodov 2013; Wadiasingh et al. 2020). This is associated with some X-ray bursts, and is consistent with observations of SGR 1935+2154 (Bochenek et al. 2020a, 2020b; Li et al. 2020; CHIME/FRB Collaboration et al. 2020; Mereghetti et al. 2020; Ridnaia et al. 2020; Scholz & Chime/Frb Collaboration 2020; Zhang et al. 2020a, 2020b). However, the luminosity of the radio burst event of SGR 1935+2154 is 1–2 orders of magnitude smaller than that inferred for typical FRBs. FRBs may have similar trigger mechanism but differ in energy budget. In general, the $E_\parallel$ proposed in most FRB models are related to the trigger mechanism, which can be revealed by observation of the time–frequency structure. Alternatively, the $E_\parallel$ in a pulsar slot gap can also accelerate the bunches of charged particles, exhibiting similar time–frequency structures.

The radio bursts of SGR 1935+2154 are separated by ∼30 ms (CHIME/FRB Collaboration et al. 2020; Scholz & Chime/Frb Collaboration 2020), which is larger than their duration. We note that there are observational differences between conventional FRBs and the radio bursts of SGR 1935+2154, but this could be the result of different activity levels in our sparking scenario, high for the former (so that charged-bunching coherent radiation beams would overlap) but low for the latter (separated by ∼30 ms). Bunches flow along neighboring field lines and emit at different heights. Therefore, one may see temporally separated sub-pulses due to the low active level and the geometric effect. The two ∼30 ms-separated peaks detected from the X-ray burst lasting 0.4 s (Li et al. 2020; Mereghetti et al. 2020; Ridnaia et al. 2020; Tavani et al. 2020; Zhang et al. 2020a, 2020b), are consistent with the separation between the CHIME events, indicative that the separated radio bursts are two sub-pulses during the 0.4 s long trigger. From another point of view, for a pulsar with spin period of ∼3 s, the angle between the magnetic axis and the

field direction of the last-open field line could be $\sim2°3$ (at an altitude of 100 km), and the time delay of two sub-pulses detected could be of order 40 ms. The sub-pulse emissions should be at least within one pulsar's period. This could be tested by future observations of periodicity if the sudden trigger can last at least one period.

For a slow rotating pulsar with an ideal dipolar configuration, the polarization angle is generally flat but evolves at near $\phi = 0$ (see Radhakrishnan & Manchester 1969). More complicated magnetic field configurations may produce more complex polarization angle evolution curves.

ORCID iDs

Wei-Yang Wang ⓘ https://orcid.org/0000-0001-9036-8543
Renxin Xu ⓘ https://orcid.org/0000-0002-9042-3044
Xuelei Chen ⓘ https://orcid.org/0000-0001-6475-8863

References

Arons, J. 1983, ApJ, 266, 215
Bassa, C. G., Tendulkar, S. P., Adams, E. A. K., et al. 2017, ApJL, 843, L8
Bannister, K. W., Deller, A. T., Phillips, C., et al. 2019, Sci, 365, 565
Beloborodov, A. M. 2013, ApJ, 777, 114
Beloborodov, A. M., & Thompson, C. 2007, ApJ, 657, 967
Bochenek, C., Kulkarni, S., Ravi, V., et al. 2020a, ATel, 13684, 1
Bochenek, C., Ravi, V., Belov, K. V., et al. 2020b, arXiv:2005.10828
Caleb, M., Stappers, B. W., Abbott, T. D., et al. 2019, arXiv:2006.08662
Chatterjee, S., Law, C. J., Wharton, R. S., et al. 2017, Natur, 541, 58
Chawla, P., Andersen, B. C., Bhardwaj, M., et al. 2020, arXiv:2004.02862
CHIME/FRB Collaboration, Amiri, M., Bandura, K., et al. 2018, ApJ, 863, 48
CHIME/FRB Collaboration, Amiri, M., Bandura, K., et al. 2019a, Natur, 566, 235
CHIME/FRB Collaboration, Andersen, B. C., Bandura, K., et al. 2019b, ApJL, 885, L24
CHIME/FRB Collaboration, Andersen, B. C., Bandura, K., et al. 2020, arXiv:2005.10324
Connor, L., Sievers, J., & Pen, U.-L. 2016, MNRAS, 458, L19
Cordes, J. M., & Wasserman, I. 2016, MNRAS, 457, 232
Dai, Z. G., Wang, J. S., Wu, X. F., & Huang, Y. F. 2016, ApJ, 829, 27
Fonseca, E., Andersen, B. C., Bhardwaj, M., et al. 2020, ApJL, 891, L6
Hessels, J. W. T., Spitler, L. G., Seymour, A. D., et al. 2019, ApJL, 876, L23
Jiang, P., Yue, Y. L., Gan, H. Q., et al. 2019, SCPMA, 62, 959502
Josephy, A., Chawla, P., Fonseca, E., et al. 2019, ApJL, 882, L18
Katz, J. I. 2014, PhRvD, 89, 103009
Katz, J. I. 2017, MNRAS, 469, L39
Keane, E. F., Stappers, B. W., Kramer, M., & Lyne, A. G. 2012, MNRAS, 425, L71
Kulkarni, S. R., Ofek, E. O., Neill, J. D., Zheng, Z., & Juric, M. 2014, ApJ, 797, 70
Kumar, P., Lu, W., & Bhattacharya, M. 2017, MNRAS, 468, 2726
Kumar, P., & Bošnjak, Ž 2020, MNRAS, 494, 2385
Li, C. K., Lin, L., Xiong, S. L., et al. 2020, arXiv:2005.11071
Lin, L., Zhang, C. F., Wang, P., et al. 2020, arXiv:2005.11479
Lorimer, D. R., Bailes, M., McLaughlin, M. A., Narkevic, D. J., & Crawford, F. 2007, Sci, 318, 777
Lu, W., & Kumar, P. 2018, MNRAS, 477, 2470
Lu, J., Peng, B., Xu, R., et al. 2019, SCPMA, 62, 959505
Lu, W., Kumar, P., & Zhang, B. 2020, arXiv:2005.06736
Luo, R., et al. 2020, Natur, submitted
Lyutikov, M. 2020, ApJ, 889, 135
Macquart, J.-P., Prochaska, J. X., McQuinn, M., et al. 2020, Natur, 581, 391
Marcote, B., Paragi, Z., Hessels, J. W. T., et al. 2017, ApJL, 834, L8
Marcote, B., Nimmo, K., Hessels, J. W. T., et al. 2020, Natur, 577, 190
Masui, K., Lin, H.-H., Sievers, J., et al. 2015, Natur, 528, 523
Mereghetti, S., Savchenko, V., Ferrigno, C., et al. 2020, arXiv:2005.06335
Muslimov, A. G., & Harding, A. K. 2004, ApJ, 606, 1143
Muslimov, A. G., & Harding, A. K. 2003, ApJ, 588, 430
Petroff, E., Johnston, S., Keane, E. F., et al. 2015, MNRAS, 454, 457
Petroff, E., Barr, E. D., Jameson, A., et al. 2016, PASA, 33, e045
Platts, E., Weltman, A., Walters, A., et al. 2019, PhR, 821, 1
Prochaska, J. X., Macquart, J.-P., McQuinn, M., et al. 2019, Sci, 366, 231
Radhakrishnan, V., & Manchester, R. N. 1969, Natur, 222, 228
Rankin, J. M. 1986, ApJ, 301, 901
Ridnaia, A., Svinkin, D., Frederiks, D., et al. 2020, arXiv:2005.11178
Ruderman, M. A., & Sutherland, P. G. 1975, ApJ, 196, 51
Ruderman, M., Zhu, T., & Chen, K. 1998, ApJ, 492, 267
Scholz, P. & Chime/Frb Collaboration 2020, ATel, 13681, 1
Spitler, L. G., Scholz, P., Hessels, J. W. T., et al. 2016, Natur, 531, 202
Tavani, M., Casentini, C., Ursi, A., et al. 2020, arXiv:2005.12164
Tendulkar, S. P., Bassa, C. G., Cordes, J. M., et al. 2017, ApJL, 834, L7
The CHIME/FRB Collaboration, Amiri, M., Andersen, B. C., et al. 2020, arXiv:2001.10275
Thompson, C., & Duncan, R. C. 1995, MNRAS, 275, 255
Thornton, D., Stappers, B., Bailes, M., et al. 2013, Sci, 341, 53
Turolla, R., Zane, S., & Drake, J. J. 2004, ApJ, 603, 265
Wadiasingh, Z., & Timokhin, A. 2019, ApJ, 879, 4
Wadiasingh, Z., Beniamini, P., Timokhin, A., et al. 2020, ApJ, 891, 82
Wang, W., Luo, R., Yue, H., et al. 2018, ApJ, 852, 140
Wang, W., Zhang, B., Chen, X., et al. 2019, ApJL, 876, L15
Xu, R. X., Qiao, G. J., & Zhang, B. 1999, ApJL, 522, L109
Yang, Y.-P., & Zhang, B. 2018, ApJ, 868, 31
Yang, Y.-P., Zhu, J.-P., Zhang, B., et al. 2020, arXiv:2006.03270
Yu, J. W., & Xu, R. X. 2011, MNRAS, 414, 489
Zhang, B. 2017, ApJL, 836, L32
Zhang, S. N., Xiong, S. L., Li, C. K., et al. 2020a, ATel, 13696, 1
Zhang, S. N., Li, C. K., Zheng, S. J., et al. 2020b, ATel, 13704, 1
Zhu, W., Li, D., Luo, R., et al. 2020, ApJL, 895, L6